

BSA-OMP: Beam-Split-Aware Orthogonal Matching Pursuit for THz Channel Estimation

Ahmet M. Elbir, *Senior Member, IEEE*, and Symeon Chatzinotas, *Fellow, IEEE*

Abstract—Terahertz (THz)-band has been envisioned for the sixth generation wireless networks thanks to its ultra-wide bandwidth and very narrow beamwidth. Nevertheless, THz-band transmission faces several unique challenges, one of which is beam-split which occurs due to the usage of subcarrier-independent analog beamformers and causes the generated beams at different subcarriers split, and point to different directions. Unlike the prior works dealing with beam-split by employing additional complex hardware components, e.g., time-delayer networks, a beam-split-aware orthogonal matching pursuit (BSA-OMP) approach is introduced to efficiently estimate the THz channel and beamformer design without any additional hardware. Specifically, we design a BSA dictionary comprised of beam-split-corrected steering vectors which inherently include the effect of beam-split so that the proposed BSA-OMP solution automatically yields the beam-split-corrected physical channel directions. Numerical results demonstrate the superior performance of BSA-OMP approach against the existing state-of-the-art techniques.

Index Terms—Terahertz, beam split, channel estimation, orthogonal matching pursuit, support recovery.

I. INTRODUCTION

Terahertz (THz) band is expected to be a key component of the sixth generation (6G) of wireless cellular networks because of its abundant available bandwidth. In particular, THz-empowered systems are envisioned to demonstrate revolutionary enhancement in the data rate ($> 100\text{Gb/s}$), extremely low latency ($< 1\text{ms}$) and ultra reliability (99.999%) [1].

Although demonstrating the aforementioned advantages, signal processing in THz band faces several THz-specific challenges that should be taken into account accordingly. These challenges include, among others, severe path loss due to spreading loss and molecular absorption, extremely-sparse path model, very short transmission distance and beam-split (see the full list in [2, 3]). In order to combat some of these challenges, e.g., path loss, analogues to massive multiple-input multiple-output (MIMO) arrays in millimeter-wave (mm-Wave) systems [4], ultra-massive MIMO architectures are envisioned, wherein subcarrier-independent analog beamformers are employed. Therefore, the directions of the generated beams at different subcarriers differentiate and point to different directions causing *beam-split* phenomenon since the analog beamformers can only be designed with respect to a single

subcarrier [5]. In mm-Wave band (0.03 – 0.3 THz), however, the subcarrier frequencies are relatively closer, and *beam-squint* is broadly used to describe the same effect [6, 7]. In comparison, the main lobes of the array gain corresponding to the lowest and highest subcarriers totally split and do not overlap while the squinted beam can still cover the entire bandwidth [8]. For instance, the amount of beam-split is approximately 6° (0.4°) for 0.3 THz with 30 GHz (60 GHz with 1 GHz) bandwidth, respectively for a broadside target (see, e.g., Fig. 1) [2].

Existing solutions to mitigate beam-split can be categorized into two classes: Hardware-based [5, 9] and algorithmic methods [8, 10–13]. The first category of solutions mainly consider employing additional hardware components such as time-delayer networks (TDNs) similar to the works studied to mitigate beam-squint [6]. The use of TDN allows the generation of a virtual beam pattern to realize a subcarrier-dependent analog beamformer to eliminate the impact of beam-split. Prior works on TDNs include the application of channel estimation [9] and hybrid precoder/combiner [5, 9] design problems. The second category, on the other hand, involves advanced signal processing techniques such as beam-split pattern detection (BSPD) [10], machine learning (ML) [11] and sparse Bayesian learning (SBL) [12]. In comparison, TDN-based approaches are cost-demanding, i.e., a single TD consumes approximately 100 mW, which is more than that of a phase shifter (40 mW) in THz [2]. Furthermore, algorithmic techniques suffer from inaccurate support estimation [10, 11], low angular precision [8, 10] and high computational complexity [8, 12, 13].

In this work, we propose an orthogonal matching pursuit (OMP)-based approach for joint THz channel and beam-split estimation. The proposed approach is advantageous since it does not require an additional hardware architecture, e.g., TDNs, and computationally-efficient because it automatically mitigates the impact of beam-split, hence called beam-split-aware OMP (BSA-OMP). In the proposed approach, beam-split is treated as an array imperfection as inspired from [12], and the beam-split-corrupted array data is transformed to beam-split-free steering vectors. Using array imperfection model, a novel BSA dictionary which inherently includes the effect of beam-split is constructed. The key idea of the BSA-OMP technique is that the amount of beam-split is known proportionally prior to THz channel estimation task, while beam-split depends on the unknown user locations. Using this observation, we construct a BSA dictionary as the set of beam-split-corrected steering vectors to generate an accurate beamspace spectra. Thus, the proposed BSA approach automatically mit-

This work was supported in part by the HORIZON Project TERRAMETA and the ERC Project AGNOSTIC.

A. M. Elbir is with the Interdisciplinary Centre for Security, Reliability and Trust (SnT) at the University of Luxembourg, Luxembourg; and Duzce University, Duzce, Turkey, (e-mail: ahmetmelbir@gmail.com).

S. Chatzinotas is with the SnT at the University of Luxembourg, Luxembourg (e-mail: symeon.chatzinotas@uni.lu).

ignates the effect of beam-split for both channel estimation and beamforming. Similar array transformation approaches have been previously investigated for mm-Wave in [8, 13]. [8] proposed an angular-delay rotation (ADR) method, which suffers from coarse beam-split estimation and high training overhead due to the use of complete discrete Fourier transform (DFT) matrix. Also, a subspace-based approach is considered in [13], which requires high training data snapshots and it may not always be applicable for THz channels in case of the highly correlated received paths. Compared to the previous works [8, 10, 13], the BSA-OMP exhibits lower computational complexity and channel overhead while accurately mitigating the beam-split.

II. WIDEBAND THZ MIMO TRANSCEIVER MODEL

Consider a wideband THz MIMO architecture with hybrid analog/digital beamforming over M subcarriers. We assume that the base station (BS) has N antennas and N_{RF} radio-frequency (RF) chains to serve K \bar{N} -antenna users. Let $\mathbf{s}[m] = [s_1[m], \dots, s_K[m]]^T$ be the vector of data symbols, where $\mathbb{E}\{\mathbf{s}[m]\mathbf{s}^H[m]\} = \frac{\rho}{K}\mathbf{I}_K$, for average power ρ and $m \in \mathcal{M} = \{1, \dots, M\}$. The data symbols are, then, processed via a $K \times K$ subcarrier-dependent baseband beamformer $\mathbf{F}_{\text{BB}}[m] = [\mathbf{f}_{\text{BB}_1}[m], \dots, \mathbf{f}_{\text{BB}_K}[m]]$. In order to steer the generated beams toward users, an $N \times N_{\text{RF}}$ subcarrier-independent analog beamformer \mathbf{F}_{RF} ($N_{\text{RF}} = K < N$) is employed. Since the analog beamformers are realized with phase-shifters, they have constant-modulus constraint, i.e., $|\mathbf{F}_{\text{RF}}[i,j]| = 1/\sqrt{\bar{N}}$ as $i = 1, \dots, N_{\text{RF}}$ and $j = 1, \dots, N$. Then, the transmitted signal, i.e., $\mathbf{F}_{\text{RF}}\mathbf{F}_{\text{BB}}[m]\mathbf{s}[m]$, is received at the k th user as

$$\tilde{\mathbf{y}}_k[m] = \mathbf{w}_{\text{RF},k}^H \mathbf{H}_k[m] \mathbf{F}_{\text{RF}} \mathbf{F}_{\text{BB}}[m] \mathbf{s}[m] + \mathbf{w}_{\text{RF},k}^H \mathbf{e}_k[m], \quad (1)$$

where $\mathbf{e}_k \in \mathbb{C}^{\bar{N}}$ is the complex additive white Gaussian noise (AWGN) vector with $\mathbf{e}_k[m] \sim \mathcal{CN}(\mathbf{0}, \mathbf{I}_{\bar{N}}\sigma_e^2)$. $\mathbf{w}_{\text{RF},k} \in \mathbb{C}^{\bar{N}}$ denotes the analog beamformer at the receiver with $|\mathbf{w}_{\text{RF},k}[n]| = 1/\sqrt{\bar{N}}$ for $n \in \{1, \dots, \bar{N}\}$.

Due to limited reflected path components and negligible scattering, the THz channel is usually constructed as the superposition of a single LoS path with a few assisting NLoS paths [3, 5, 7]. In addition, multipath channel models are also widely used, especially for indoor applications [3, 14]. Hence, we consider a general scenario, wherein the $\bar{N} \times N$ channel matrix is represented by the combination of L paths with physical direction-of-arrival (DOA) and direction-of-departure (DOD) angles $\phi_{k,l} = \sin \tilde{\phi}_{k,l}$ and $\varphi_{k,l} = \sin \tilde{\varphi}_{k,l}$ ($\tilde{\phi}_{k,l}, \tilde{\varphi}_{k,l} \in [-\frac{\pi}{2}, \frac{\pi}{2}]$), respectively [3]. Due to wideband processing, beam-split occurs and the physical directions ($\phi_{k,l}, \varphi_{k,l}$) are deviated in spatial domain ($\theta_{k,m,l}, \vartheta_{k,m,l}$). We define the corresponding subcarrier-dependent spatial directions explicitly as

$$\theta_{k,m,l} = \frac{f_m}{f_c} \phi_{k,l} = \eta_m \phi_{k,l}, \vartheta_{k,m,l} = \frac{f_m}{f_c} \varphi_{k,l} = \eta_m \varphi_{k,l}, \quad (2)$$

where $f_m = f_c + \frac{B}{M}(m-1 - \frac{M-1}{2})$ for f_c and B being the carrier frequency and bandwidth, respectively. $\eta_m = \frac{f_m}{f_c}$, c_0

is speed of light and $d = \frac{c_0}{2f_c}$ is the array element spacing. Now, we can introduce the $\bar{N} \times N$ channel matrix as

$$\mathbf{H}_k[m] = \zeta \sum_{l=1}^L \alpha_k \bar{\mathbf{a}}(\theta_{k,m,l}) \mathbf{a}^H(\vartheta_{k,m,l}) e^{-j2\pi\tau_{k,l}f_m}, \quad (3)$$

where $\zeta = \sqrt{\bar{N}N/L}$, $\alpha_k \in \mathbb{C}$ is the complex path gain and $\tau_{k,l}$ represents the time delay of the l th path corresponding to the array origin. $\bar{\mathbf{a}}(\theta_{k,m,l}) \in \mathbb{C}^{\bar{N}}$ and $\mathbf{a}(\vartheta_{k,m,l}) \in \mathbb{C}^N$ are the beam-split-corrupted subcarrier-dependent actual array steering vectors corresponding to spatial DOA/DOD angles. In particular, using (2), $\bar{\mathbf{a}}(\theta_{k,m,l})$ can be defined in terms of the physical DOA $\phi_{k,l}$ for uniform linear array (ULA) as

$$\bar{\mathbf{a}}(\theta_{k,m,l}) = [1, e^{-j\pi\eta_m\phi_{k,l}}, \dots, e^{-j\pi(\bar{N}-1)\eta_m\phi_{k,l}}]^T, \quad (4)$$

for which we can define $\mathbf{a}(\vartheta_{k,m,l})$ similarly in terms of $\varphi_{k,l}$.

III. PROPOSED METHOD

In mm-Wave systems, the subcarrier-frequencies are close to each other, i.e., $f_{m_1} \approx f_{m_2}, \forall m_1, m_2 \in \mathcal{M}$, which allows one to employ a single operating wavelength, i.e., $\lambda_1 = \dots = \lambda_M = \frac{c_0}{f_c}$, for the design of analog beamformers [4, 6, 15]. However, this causes deviations in the direction of the generated beams, especially at the far end subcarriers. Although this deviations might be tolerable in mm-Wave [4, 15], in THz-band, the bandwidth is so wide that a single-wavelength assumption for analog beamforming cannot hold and it leads to the split of physical directions, which are observed as spatial directions in the beamspace.

A. Beam-Split Model

Using (2) and (4), we first rewrite the n th element of beam-split-corrupted steering vector $\bar{\mathbf{a}}(\theta_{k,m,l})$ as

$$[\bar{\mathbf{a}}(\theta_{k,m,l})]_n = e^{-j\pi(n-1)\theta_{k,m,l}} = e^{-j\pi(n-1)\eta_m\phi_{k,l}}, \quad (5)$$

while the beam-split-free steering vector element is formulated as $[\bar{\mathbf{a}}(\phi_{k,l})]_n = e^{-j\pi(n-1)\phi_{k,l}}$, and we define

$$\Delta_{k,l}[m] = \theta_{k,m,l} - \phi_{k,l} = (\eta_m - 1)\phi_{k,l}, \quad (6)$$

as beam-split to design BSA dictionary in the following.

Proposition 1. *Let $\bar{\mathbf{a}}(\theta_{k,m,l})$ and $\bar{\mathbf{a}}(\phi_{k,l})$ be the steering vectors corresponding to spatial and physical DOAs, respectively. Then, the linear transformation*

$$\bar{\mathbf{a}}(\theta_{k,m,l}) = \mathbf{\Gamma}(\theta_{k,m,l})\bar{\mathbf{a}}(\phi_{k,l}), \quad (7)$$

holds for $\mathbf{\Gamma}(\theta_{k,m,l}) = \text{diag}\{\gamma(\theta_{k,m,l})\} \in \mathbb{C}^{\bar{N} \times \bar{N}}$, where $\gamma(\theta_{k,m,l}) = [\gamma_1(\theta_{k,m,l}), \dots, \gamma_{\bar{N}}(\theta_{k,m,l})]^T$ and $\gamma_n(\theta_{k,m,l}) = e^{-j\pi(n-1)\Delta_{k,l}[m]}$.

Proof: The n th element of $\bar{\mathbf{a}}(\theta_{k,m,l})$ and $\bar{\mathbf{a}}(\phi_{k,l})$ can be written as $[\bar{\mathbf{a}}(\theta_{k,m,l})]_n = e^{-j\pi(n-1)\theta_{k,m,l}}$ and $[\bar{\mathbf{a}}(\phi_{k,l})]_n = e^{-j\pi(n-1)\phi_{k,l}}$, respectively. By using (6), $\gamma_n(\theta_{k,m,l})$ can be obtained from $\gamma_n(\theta_{k,m,l}) = \frac{[\bar{\mathbf{a}}(\theta_{k,m,l})]_n}{[\bar{\mathbf{a}}(\phi_{k,l})]_n}$ as $\gamma_n(\theta_{k,m,l}) = e^{-j\pi(n-1)(\theta_{k,m,l} - \phi_{k,l})} = e^{-j\pi(n-1)\Delta_{k,l}[m]}$. ■

Note that the aforementioned analysis can also be done for $\mathbf{a}(\varphi)$, and the structure of $\mathbf{\Gamma}_m(\phi_{k,l})$ allows us to estimated the beam-split at the m th subcarrier as discussed below.

Corollary 1. Given $\Gamma_m(\phi_{k,l})$, the beam-split introduced at the m th subcarrier can be uniquely obtained via [12]

$$\Delta_{k,l}[m] = \frac{1}{\bar{N}-1} \sum_{n=2}^{\bar{N}} \frac{\angle\{\gamma(\theta_{k,m,l})\}_n}{\pi(n-1)}. \quad (8)$$

Proof: The n th entry of $\bar{\mathbf{a}}(\theta_{k,m,l})$ is given by $[\bar{\mathbf{a}}(\theta_{k,m,l})]_n = e^{-j\pi(n-1)\theta_{k,m,l}}$, whose angle is computed as $\Omega_{k,l,n}[m] = \angle[\bar{\mathbf{a}}(\theta_{k,m,l})]_n = -\pi(n-1)\theta_{k,m,l}$ for $n = 1, \dots, \bar{N}$. Next, we compute the unwrapped angles as $\Omega_{k,l}[m] = \text{unwrap}\{\Omega_{k,l,1}[m], \dots, \Omega_{k,l,\bar{N}}[m]\}^T$. Using $\Omega_k[m]$, the n th element of $\bar{\mathbf{a}}(\phi_{k,l})$ becomes $[\bar{\mathbf{a}}(\theta_{k,m,l})]_n = e^{-j\frac{\Omega_{k,l,n}[m]}{\eta_m}}$. Substituting $[\bar{\mathbf{a}}(\theta_{k,m,l})]_n$ into (7) yields $\gamma_n(\theta_{k,m,l}) = \frac{[\bar{\mathbf{a}}(\theta_{k,m,l})]_n}{[\bar{\mathbf{a}}(\phi_{k,l})]_n}$, and we get

$$\begin{aligned} \angle\{\gamma_n(\theta_{k,m,l})\} &= \Omega_{k,l,n}[m] - \frac{\Omega_{k,l,n}[m]}{\eta_m} = \Omega_{k,l,n}[m] \frac{\eta_m - 1}{\eta_m} \\ &= \pi(n-1)\theta_{k,m,l} \left(\frac{\theta_{k,m,l} - \phi_{k,l}}{\theta_{k,m,l}} \right) = \pi(n-1)\Delta_{k,l}[m]. \end{aligned} \quad (9)$$

Taking average of $\angle\{\gamma_n(\theta_{k,m,l})\}$ for $n = 2, \dots, \bar{N}$ yields

$$\frac{1}{\bar{N}-1} \sum_{n=2}^{\bar{N}} \angle\{\gamma_n(\theta_{k,m,l})\} = \pi(n-1)\Delta_{k,l}[m]. \quad (10)$$

By dividing both sides by $\pi(n-1)$ in (10), we get $\Delta_{k,l}[m]$. ■

B. BSA Dictionary Design

We design a BSA dictionary whose columns are constructed according to the directions that are affected by beam-split. Hence, for an arbitrary physical directions $\phi_{k,l}, \varphi_{k,l} \in [-1, 1]$, we can readily compute the spatial directions as $\eta_m\phi_{k,l}, \eta_m\varphi_{k,l}$. Using this observation, we design the BSA dictionaries $\bar{\mathbf{C}}_m, \mathbf{C}_m$ composed of steering vectors $\mathbf{c}(\theta_m) \in \mathbb{C}^{\bar{N}}, \bar{\mathbf{c}}(\vartheta_m) \in \mathbb{C}^{\bar{N}}$ as

$$\begin{aligned} \bar{\mathbf{C}}_m &= \{\bar{\mathbf{c}}(\theta_m) | \bar{\mathbf{c}}(\theta_m) \triangleq \Gamma(\theta_m)\bar{\mathbf{a}}(\phi), \theta_m \in [-\eta_m, \eta_m]\}, \\ \mathbf{C}_m &= \{\mathbf{c}(\vartheta_m) | \mathbf{c}(\vartheta_m) \triangleq \Gamma(\vartheta_m)\mathbf{a}(\varphi), \vartheta_m \in [-\eta_m, \eta_m]\}. \end{aligned}$$

Using the BSA dictionaries, one can readily obtain the physical directions as $\phi = \theta_m/\eta_m$ and $\varphi = \vartheta_m/\eta_m, \forall m \in \mathcal{M}$.

C. Channel Estimation

In downlink, the channel estimation stage is performed simultaneously by all the users during channel training. Since the BS employs hybrid beamforming architecture, it activates only a single RF chain in each channel use to transmit the pilot signals during channel acquisition [4, 15]. Hence, the BS employs P beamformer vectors as $\bar{\mathbf{F}} = [\bar{\mathbf{f}}_1, \dots, \bar{\mathbf{f}}_P] \in \mathbb{C}^{\bar{N} \times P}$ ($|\bar{\mathbf{f}}_p| = 1/\sqrt{\bar{N}}$) to send P orthogonal pilot signals, $\bar{\mathbf{S}} = \text{diag}\{\bar{s}_1, \dots, \bar{s}_P\} \in \mathbb{C}^{P \times P}$. For each pilot, the users employ \bar{P} combining vectors $\bar{\mathbf{W}} = [\bar{\mathbf{w}}_1, \dots, \bar{\mathbf{w}}_{\bar{P}}] \in \mathbb{C}^{\bar{N} \times \bar{P}}$ ($|\bar{\mathbf{w}}_p| = 1/\sqrt{\bar{N}}$) in each channel use. Hence, the total channel

¹The unwrapping operation is necessary to ensure not losing information due to $[-\pi, \pi]$ periodicity of the exponential (i.e., $|(n-1)\theta_{k,m,l}| > 1$), which is ignored in the previous works [8, 13].

Algorithm 1 BSA-OMP for channel estimation

Input: $\mathbf{Y}_k[m], \mathbf{G}_m$ and $\eta_m, \forall m \in \mathcal{M}$.
Output: Channel estimate $\hat{\mathbf{H}}_k[m]$, beam-split $\hat{\Delta}_{k,l}[m]$.

- 1: **for** $k \in \mathcal{K}$
- 2: $l = 1, \bar{\mathcal{I}}_{l-1} = \mathcal{I}_{l-1} = \emptyset, \mathbf{r}_{l-1}[m] = \mathbf{y}_k[m], \forall m \in \mathcal{M}$.
- 3: **while** $l \leq L$ **do**
- 4: $\{\bar{q}^*, q^*\} = \text{argmax}_{\bar{q}, q} \sum_{m=1}^M |\psi_{\bar{q}, q}^H[m] \mathbf{r}_{l-1}[m]|$,
 where $\psi_{\bar{q}, q}[m] = (\bar{\mathbf{F}}^T \mathbf{c}^*(\theta_{m,q})) \otimes (\bar{\mathbf{W}}^H \bar{\mathbf{c}}(\vartheta_{m,\bar{q}}))$.
- 5: $\bar{\mathcal{I}}_l = \bar{\mathcal{I}}_{l-1} \cup \{\bar{q}^*\}, \hat{\phi}_{k,l} = \frac{\theta_{m,\bar{q}^*}}{\eta_m}$.
- 6: $\mathcal{I}_l = \mathcal{I}_{l-1} \cup \{q^*\}, \hat{\varphi}_{k,l} = \frac{\vartheta_{m,q^*}}{\eta_m}$.
- 7: $\hat{\Delta}_{k,l}[m] = \hat{\theta}_{m,\bar{q}^*} - \hat{\phi}_{k,l}, \forall m \in \mathcal{M}$.
- 8: $\Psi_m(\mathcal{I}_l) = (\bar{\mathbf{F}}^T \mathbf{C}_m(\mathcal{I}_l)) \otimes (\bar{\mathbf{W}}^H \bar{\mathbf{C}}(\bar{\mathcal{I}}_l))$.
- 9: $\mathbf{r}_l[m] = (\mathbf{I}_{\bar{P}P} - \Psi_m(\mathcal{I}_l) \Psi_m^\dagger(\mathcal{I}_l)) \mathbf{y}_k[m]$.
- 10: $l = l + 1$.
- 11: **end while**
- 12: $\bar{\Xi}_k = [\bar{\mathbf{a}}(\hat{\phi}_{k,1}), \dots, \bar{\mathbf{a}}(\hat{\phi}_{k,L})], \Xi_k = [\mathbf{a}(\hat{\varphi}_{k,1}), \dots, \mathbf{a}(\hat{\varphi}_{k,L})]$.
- 13: **for** $m \in \mathcal{M}$
- 14: $\hat{\mathbf{z}}_k[m] = \Psi_m^\dagger(\mathcal{I}_{l-1}) \mathbf{y}_k[m]$.
- 15: $\hat{\mathbf{H}}_k[m] = \bar{\Xi}_k \text{diag}\{\hat{\mathbf{z}}_k[m]\} \Xi_k^H$.
- 16: **end for**
- 17: **end for**

use for processing all pilots is $P\bar{P}$. Then, the pilot signals are collected by the k th receiver in a $\bar{P} \times P$ matrix as

$$\mathbf{Y}_k[m] = \bar{\mathbf{W}}^H \mathbf{H}_k[m] \bar{\mathbf{F}} \bar{\mathbf{S}} + \bar{\mathbf{E}}_k[m], \quad (11)$$

where $\bar{\mathbf{E}}_k[m] = \bar{\mathbf{W}}^H \mathbf{E}_k[m]$ is the effective noise term. Assuming $\bar{\mathbf{S}} = \mathbf{I}_P$, we get $\mathbf{Y}_k[m] = \bar{\mathbf{W}}^H \mathbf{H}_k[m] \bar{\mathbf{F}} + \bar{\mathbf{E}}_k[m]$, which can be written in a vector form as

$$\mathbf{y}_k[m] = \mathbf{G} \mathbf{h}_k[m] + \tilde{\mathbf{e}}_k[m], \quad (12)$$

where $\mathbf{y}_k[m] = \text{vec}\{\mathbf{Y}_k[m]\} \in \mathbb{C}^{P\bar{P}}, \mathbf{G} = \bar{\mathbf{F}}^T \otimes \bar{\mathbf{W}}^H \in \mathbb{C}^{P\bar{P} \times \bar{N}N}, \mathbf{h}_k[m] = \text{vec}\{\mathbf{H}_k[m]\}, \tilde{\mathbf{e}}_k[m] = \text{vec}\{\bar{\mathbf{E}}_k[m]\}$, where \otimes denotes the Kronecker product. By exploiting the THz channel sparsity, (12) is rewritten as

$$\mathbf{y}_k[m] = \Psi_m \mathbf{x}_k[m] + \tilde{\mathbf{e}}_k[m], \quad (13)$$

where $\Psi_m = (\bar{\mathbf{F}}^T \mathbf{C}_m^*) \otimes (\bar{\mathbf{W}}^H \bar{\mathbf{C}}_m) \in \mathbb{C}^{P\bar{P} \times Q^2}$, for which $\bar{\mathbf{C}}_m = [\bar{\mathbf{c}}(\theta_{m,1}), \dots, \bar{\mathbf{c}}(\theta_{m,Q})]$ and $\mathbf{C}_m = [\mathbf{c}(\vartheta_{m,1}), \dots, \mathbf{c}(\vartheta_{m,Q})]$ are the $\bar{N} \times Q$ and $N \times Q$ dictionary matrices covering the spatial domain with $\theta_{m,q}, \vartheta_{m,q} \in [-\eta_m, \eta_m]$ ($\phi, \varphi \in [-1, 1]$) for $q = 1, \dots, Q$ as defined in Sec. III-B. $\mathbf{x}_k[m] \in \mathbb{C}^{Q^2}$ is an L -sparse vector, whose non-zero elements corresponds to the set $\{z_{k,l}[m] | z_{k,l}[m] \triangleq \zeta \alpha_k e^{-j2\pi\tau_{k,l} f_m}, l = 1, \dots, L\}$.

Using the BSA dictionaries, we can employ OMP algorithm to jointly estimate the THz channel support and the beam-split [9, 10]. The proposed BSA-OMP technique is presented in Algorithm 1, wherein the physical angles and beam-split are obtained for $m \in \mathcal{M}$ (Step 3 – 11). Then, the estimated THz channel $\hat{\mathbf{H}}_k[m]$ is constructed from the set of steering vectors of physical DOAs (Step 12 – 17).

D. Beamformer Design

Once the channel is estimated, it is used to design the hybrid beamformers $\mathbf{F}_{\text{RF}}, \mathbf{F}_{\text{BB}}[m]$ and $\mathbf{W}_{\text{RF}} =$

$[\mathbf{w}_{\text{RF},1}, \dots, \mathbf{w}_{\text{RF},K}]$ via maximizing the overall spectral efficiency. The design problem is equivalent to maximizing $\sum_{m=1}^M |\mathbf{u}_{q,\bar{q}}^H[m] \mathbf{v}_k[m]|$, which is the correlation cost between the hybrid and unconstrained beamformers $\mathbf{F}_{\text{opt}}[m] \in \mathbb{C}^{N \times K}$ and $\mathbf{W}_{\text{opt}}[m] \in \mathbb{C}^{\bar{N} \times K}$ [4]. Here, $\mathbf{u}_{q,\bar{q}}[m]$ denotes the BSA dictionary columns as $\mathbf{u}_{q,\bar{q}}[m] = [\mathbf{C}_m]_{q,\bar{q}}^* \otimes [\bar{\mathbf{C}}_m]_{q,\bar{q}} \in \mathbb{C}^{\bar{N}N}$ and $\mathbf{v}_k[m] = \mathbf{f}_{\text{opt},k}^*[m] \otimes \mathbf{w}_{\text{opt},k}[m] \in \mathbb{C}^{\bar{N}N}$ corresponds to the unconstrained beamformers, wherein $\mathbf{f}_{\text{opt},k}[m]$ can be obtained from the singular value decomposition (SVD) of $\mathbf{H}_k[m]$ [4], and $\mathbf{w}_{\text{opt},k}[m] = \frac{1}{\rho} (\mathbf{f}_{\text{opt},k}^H[m] \mathbf{H}_k^H[m] \mathbf{H}_k[m] \mathbf{f}_{\text{opt},k}[m] + \frac{\sigma_w^2}{\rho})^{-1} \mathbf{f}_{\text{opt},k}^H[m] \mathbf{H}_k[m]$. Next, we find the k th column of the analog beamformers from

$$\{q^*, \bar{q}^*\} = \underset{q, \bar{q}}{\operatorname{argmax}} \sum_{m=1}^M |\mathbf{u}_{q,\bar{q}}^H[m] \mathbf{v}_k[m]|, \quad (14)$$

where $\{q^*, \bar{q}^*\}$ denote the selected beamformer indices. Then, the k th column of \mathbf{F}_{RF} and \mathbf{W}_{RF} are selected from the steering vectors corresponding to the physical directions as $\mathbf{a}(\phi_{q^*})$ and $\bar{\mathbf{a}}(\varphi_{\bar{q}^*})$, respectively. In order to mitigate the inter-user interference, the baseband beamformer is obtained from the $K \times K$ effective channel matrix whose the k th column is $[\mathbf{H}_{\text{eff}}[m]]_k = \mathbf{w}_{\text{RF},k}^H \mathbf{H}_k[m] \mathbf{F}_{\text{RF}}$, $k \in \mathcal{K}$, and the baseband beamformer is computed as $\mathbf{F}_{\text{BB}}[m] = \mathbf{H}_{\text{eff}}[m]^\dagger$. The algorithmic steps of the proposed BSA-OMP approach for beamformer design are presented in Algorithm 2.

E. Complexity and Training Overhead

The computational complexity of proposed BSA-OMP approaches is the same as traditional OMP techniques [4]. In particular, the complexity of the BSA-OMP approach for channel estimation in Algorithm 1 is mainly due to the matrix multiplications in step 4 ($O(M(3P\bar{P} + PN^2 + \bar{P}\bar{N}^2))$), step 8 ($O(2P\bar{P}L)$) and step 14 ($O(P^3\bar{P}^3 + LP^2\bar{P}^2 + LP\bar{P})$). The channel training complexity of the proposed BSA-OMP approach requires only $P\bar{P}$ (16 times lower, see Sec. IV) channel use for pilot signaling while the tradition approaches, e.g., LS, MMSE and ADR [8], need at least $N\bar{N}$ channel use.

The complexity of the proposed beamforming approach in Algorithm 2 is mainly due to operations in steps 3 – 4 with total complexity of $O(K(N + \bar{N}) + MN\bar{N})$. Furthermore, the proposed approach does not require additional hardware components as opposed to the previous works employing TDNs [5, 6, 9].

IV. NUMERICAL EXPERIMENTS

Throughout the simulations (unless stated otherwise), the signal model in (3) is generated with $f_c = 300$ GHz, $B = 30$ GHz, $M = 128$, $N = 256$, $\bar{N} = 16$, $P = \bar{P} = 16$, $N_{\text{RF}} = 8$, $L = 3$, $K = 8$, $Q = 8N$ [3, 5]. The beamformer matrices $\tilde{\mathbf{F}}$ and $\tilde{\mathbf{W}}$ are modeled with random phases as $[\tilde{\mathbf{F}}]_{i,j} \frac{1}{\sqrt{N}} e^{j\psi_F}$, $[\tilde{\mathbf{W}}]_{i,j} \frac{1}{\sqrt{\bar{N}}} e^{j\psi_W}$, where $\psi_F, \psi_W \sim \text{uniform}[-\frac{\pi}{2}, \frac{\pi}{2}]$.

Fig. 1 shows the array gain with respect to physical DOA of a single user scenario. In Fig. 1(a)-(b), array gain is computed for the user physical DOA at 30° and 60° for all subcarriers when $M = 15$. We can see significant deviation in the beamspace due to beam-split, which is about 3° (6°)

Algorithm 2 BSA-OMP for hybrid beamforming

-
- Input:** $\bar{\mathbf{C}}_m, \mathbf{C}_m, \mathbf{F}_{\text{opt}}[m], \mathbf{W}_{\text{opt}}[m], \eta_m, m \in \mathcal{M}$.
Output: $\mathbf{F}_{\text{RF}}, \mathbf{F}_{\text{BB}}[m], \mathbf{W}_{\text{RF}}$.
- 1: $\mathbf{F}_{\text{RF}} = \emptyset, \mathbf{F}_r[m] = \mathbf{F}_{\text{opt}}[m],$
 $\mathbf{W}_{\text{RF}} = \emptyset, \mathbf{W}_r[m] = \mathbf{W}_{\text{opt}}[m].$
 - 2: **for** $k = 1, \dots, N_{\text{RF}}$ **do**
 - 3: $\mathbf{v}_k[m] = \mathbf{f}_{r,k}^*[m] \otimes \mathbf{w}_{r,k}[m], m \in \mathcal{M}.$
 - 4: $\{q^*, \bar{q}^*\} = \operatorname{argmax}_{q, \bar{q}} \sum_{m=1}^M |\mathbf{u}_{q,\bar{q}}^H[m] \mathbf{v}_k[m]|.$
 - 5: $\mathbf{F}_{\text{RF}} = [\mathbf{F}_{\text{RF}} | \mathbf{a}(\phi_{q^*})], \mathbf{W}_{\text{RF}} = [\mathbf{W}_{\text{RF}} | \bar{\mathbf{a}}(\varphi_{\bar{q}^*})].$
 - 6: **end for**
 - 7: $[\mathbf{H}_{\text{eff}}[m]]_k = \mathbf{w}_{\text{RF},k}^H \mathbf{H}_k[m] \mathbf{F}_{\text{RF}}, k \in \mathcal{K}.$
 - 8: $\mathbf{F}_{\text{BB}}[m] = \mathbf{H}_{\text{eff}}[m]^\dagger, m \in \mathcal{M}.$
 - 9: $[\mathbf{F}_{\text{BB}}[m]]_k = [\mathbf{F}_{\text{BB}}[m]]_k / \|\mathbf{F}_{\text{RF}} \mathbf{F}_{\text{BB}}[m]\|_{\mathcal{F}}, k \in \mathcal{K}.$
-

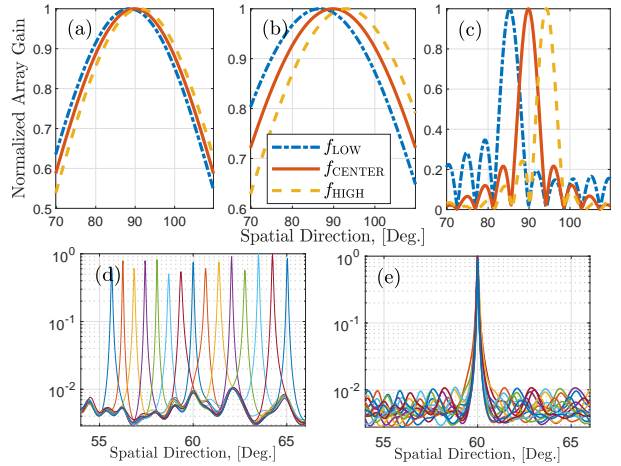


Fig. 1. Array gain with respect to spatial direction at low, center and high end subcarriers for (a) $f_c = 3.5$ GHz, $B = 0.1$ GHz; (b) $f_c = 28$ GHz, $B = 2$ GHz; and (c) $f_c = 300$ GHz, $B = 30$ GHz, respectively. Array gain corresponding to the all subcarriers (d) under the effect of beam-split and (e) the beam-split-corrected array gain by using BSA-OMP.

for the physical DOA 30° (60°), respectively. The array gain computed by using the proposed BSA approach is also given in Fig. 1(c)-(d), respectively. As it is seen, the proposed BSA approach effectively mitigates the impact of beam-split and the spectra of all subcarriers align toward the same (physical channel) direction.

In Fig. 2, THz channel estimation performance of the proposed BSA-OMP approach is evaluated, in comparison with the state-of-the-art techniques, OMP [15], least-squares (LS), oracle LS (OLS), minimum mean-squared-error (MMSE), generalized simultaneous OMP (GSOMP) [9], ADR [8], BSPD [10], in terms of normalized MSE of the channel: $\text{NMSE} = \frac{\|\mathbf{h}_k[m] - \hat{\mathbf{h}}_k[m]\|_2^2}{\|\mathbf{h}_k[m]\|_2^2}$ against signal-to-noise ratio (SNR). Note that the MMSE estimator relies on the true covariance matrix and it is computed for each subcarrier exclusively, hence it is regarded as the benchmark method in this work. We can see from Fig. 2 that poor performance is achieved by the conventional techniques, e.g., OMP, LS and OLS, that do not take into account the effect of beam-split. Although

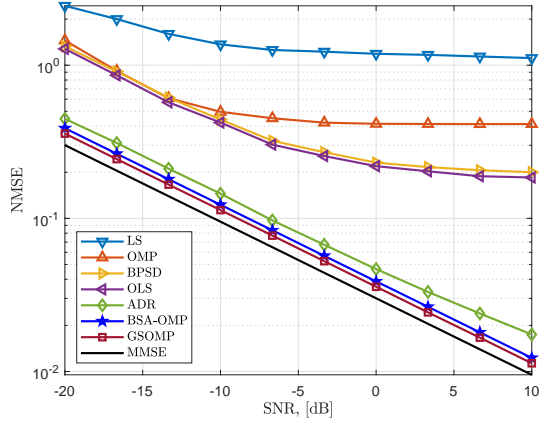


Fig. 2. THz wideband channel estimation, NMSE versus SNR.

ADR employs an angular rotation to mitigate the beam-split, it encounters error floors at high SNR regions due the use of coarse beam-split estimation and low resolution Fourier dictionary. Similarly, BSPD uses a beam-split detection mechanism, it fails to recover the channel supports accurately. On the other hand, the proposed BSA-OMP approach achieves much better performance compared to aforementioned techniques and attain a close performance to MMSE and GSOMP, which employs additional hardware components, i.e., TDNs, to mitigate beam-split. In contrast, our BSA-OMP approach does not require TDN, hence, it is more hardware-efficient while maintaining sufficient NMSE performance.

Fig.3 shows the hybrid beamforming performance in terms of sum-rate, wherein the unconstrained beamformers, i.e., $\mathbf{F}_{\text{opt}}[m]$, $\mathbf{W}_{\text{opt}}[m]$, are employed for fully-digital beamformer as a benchmark. A significant performance improvement is observed when the proposed BSA approach is applied to the traditional OMP technique [4], which does not take into account the effect of beam-split. The proposed method is also superior than the delay-phase precoding (DPP) method [16], which employs a TDN to realize frequency-dependent analog beamformer while no such requirement is needed for BSA-OMP.

V. SUMMARY

In this work, we introduced a BSA-OMP approach to effectively mitigate the effect of beam-split for THz channel estimation and beamforming. Compared to prior works, the proposed approach is advantageous since it does not require additional hardware components, e.g., TDNs, while maintaining close-to-MMSE (fully-digital) channel estimation (beamforming) performance. Furthermore, the complexity of BSA-OMP is low and the same as for the traditional OMP technique.

REFERENCES

[1] T. S. Rappaport, Y. Xing, O. Kanhere, S. Ju, A. Madanayake, S. Mandal, A. Alkhateeb, and G. C. Trichopoulos, "Wireless Communications and Applications Above 100 GHz: Opportunities and Challenges for 6G and Beyond," *IEEE Access*, vol. 7, pp. 78 729–78 757, Jun. 2019.

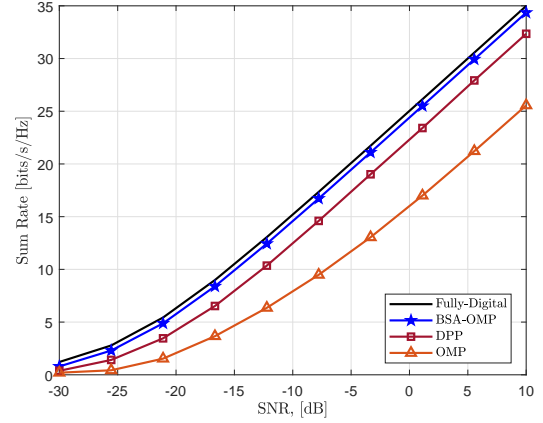


Fig. 3. THz wideband hybrid beamforming, sum-rate versus SNR.

[2] A. M. Elbir, K. V. Mishra, S. Chatzinotas, and M. Bennis, "Terahertz-Band Integrated Sensing and Communications: Challenges and Opportunities," *arXiv preprint arXiv:2208.01235*, Aug. 2022.

[3] H. Sarrideen, M.-S. Alouini, and T. Y. Al-Naffouri, "An overview of signal processing techniques for Terahertz communications," *Proceedings of the IEEE*, vol. 109, no. 10, pp. 1628–1665, 2021.

[4] R. W. Heath, N. González-Prelcic, S. Rangan, W. Roh, and A. M. Sayeed, "An Overview of Signal Processing Techniques for Millimeter Wave MIMO Systems," *IEEE J. Sel. Top. Signal Process.*, vol. 10, no. 3, pp. 436–453, Feb. 2016.

[5] J. Tan and L. Dai, "Wideband Beam Tracking in THz Massive MIMO Systems," *IEEE J. Sel. Areas Commun.*, vol. 39, no. 6, pp. 1693–1710, Apr 2021.

[6] B. Wang, M. Jian, F. Gao, G. Y. Li, and H. Lin, "Beam Squint and Channel Estimation for Wideband mmWave Massive MIMO-OFDM Systems," *IEEE Trans. Signal Process.*, vol. 67, no. 23, pp. 5893–5908, Oct. 2019.

[7] A. M. Elbir, K. V. Mishra, and S. Chatzinotas, "Terahertz-Band Joint Ultra-Massive MIMO Radar-Communications: Model-Based and Model-Free Hybrid Beamforming," *IEEE J. Sel. Top. Signal Process.*, vol. 15, no. 6, pp. 1468–1483, Oct. 2021.

[8] B. Wang, F. Gao, S. Jin, H. Lin, and G. Y. Li, "Spatial- and Frequency-Wideband Effects in Millimeter-Wave Massive MIMO Systems," *IEEE Trans. Signal Process.*, vol. 66, no. 13, pp. 3393–3406, May 2018.

[9] K. Dovelos, M. Matthaiou, H. Q. Ngo, and B. Bellalta, "Channel Estimation and Hybrid Combining for Wideband Terahertz Massive MIMO Systems," *IEEE J. Sel. Areas Commun.*, vol. 39, no. 6, pp. 1604–1620, Apr. 2021.

[10] J. Tan and L. Dai, "Wideband channel estimation for THz massive MIMO," *China Commun.*, vol. 18, no. 5, pp. 66–80, May 2021.

[11] A. M. Elbir, W. Shi, K. V. Mishra, and S. Chatzinotas, "Federated Multi-Task Learning for THz Wideband Channel and DoA Estimation," *arXiv preprint arXiv:2207.06017*, Jul. 2022.

[12] A. M. Elbir, W. Shi, A. K. Papazafeiropoulos, P. Kourtessis, and S. Chatzinotas, "Terahertz-Band Channel and Beam Split Estimation via Array Perturbation Model," *arXiv preprint arXiv:2208.03683*, Aug. 2022.

[13] J. P. González-Coma, P. Suárez-Casal, P. M. Castro, and L. Castedo, "FDD Channel Estimation Via Covariance Estimation in Wideband Massive MIMO Systems," *Sensors*, vol. 20, no. 3, p. 930, Feb. 2020.

[14] S. Tarboush, H. Sarrideen, H. Chen, M. H. Loukil, H. Jemaa, M. S. Alouini, and T. Y. Al-Naffouri, "TeraMIMO: A Channel Simulator for Wideband Ultra-Massive MIMO Terahertz Communications," *arXiv*, Apr 2021.

[15] J. Rodríguez-Fernández, N. González-Prelcic, K. Venugopal, and R. W. Heath, "Frequency-Domain Compressive Channel Estimation for Frequency-Selective Hybrid Millimeter Wave MIMO Systems," *IEEE Trans. Wireless Commun.*, vol. 17, no. 5, pp. 2946–2960, Mar. 2018.

[16] L. Dai, J. Tan, Z. Chen, and H. V. Poor, "Delay-Phase Precoding for Wideband THz Massive MIMO," *IEEE Trans. Wireless Commun.*, p. 1, Mar. 2022.